Geophysical Research Letters

RESEARCH LETTER
10.1029/2025GL116503

Temporarily Increased Recurrence Rate of Shallow Slow Slip Events Driven by Significant Afterslip Following the 2012 M_w 7.6 Nicoya Earthquake

Guoli Li[1], Surui Xie[1], Marino Protti[2], and Cyril Muller[2]

[1]Department of Civil and Environmental Engineering, University of Houston, Houston, TX, USA, [2]Observatorio Vulcanológico y Sismológico de Costa Rica, Universidad Nacional, Heredia, Costa Rica

Key Points:

- More frequent shallow slow slip events (SSEs) occurred several months after the 2012 M_w 7.6 Nicoya earthquake
- The area of more frequent shallow SSEs is immediately next to the updip edge of the largest afterslip zone
- The increase of shallow SSE frequency is caused by afterslip through Coulomb stress change

Supporting Information:

Supporting Information may be found in the online version of this article.

Correspondence to:

G. Li,
gli19@uh.edu

Citation:

Li, G., Xie, S., Protti, M., & Muller, C. (2025). Temporarily increased recurrence rate of shallow slow slip events driven by significant afterslip following the 2012 M_w 7.6 Nicoya earthquake. *Geophysical Research Letters*, *52*, e2025GL116503. https://doi.org/10.1029/2025GL116503

Received 14 APR 2025
Accepted 1 SEP 2025

Author Contributions:

Conceptualization: Surui Xie
Data curation: Surui Xie
Formal analysis: Guoli Li
Funding acquisition: Surui Xie, Marino Protti, Cyril Muller
Investigation: Guoli Li
Methodology: Surui Xie
Project administration: Surui Xie
Resources: Surui Xie, Marino Protti, Cyril Muller
Software: Guoli Li
Supervision: Surui Xie
Visualization: Guoli Li
Writing – original draft: Guoli Li
Writing – review & editing: Surui Xie, Marino Protti, Cyril Muller

Abstract Slow slip events (SSEs) release tectonic strain without causing sudden ground shaking. SSEs have been observed at many subduction zones, some dynamically triggered by stress changes due to the passage of seismic waves. However, there are limited observations of SSEs induced by post-seismic deformation. Here, we report a significant increase in the recurrence rate of SSEs in the shallow portion of the Nicoya megathrust following the 2012 M_w 7.6 earthquake. These shallow SSEs occurred immediately updip of the large afterslip zone and their recurrence rate returned to pre-earthquake level 1.5 years after the earthquake. In contrast, deeper SSE recurrence rate remained unchanged. Coulomb Failure Stress modeling indicates the shallow SSE area experienced substantial stress perturbation during afterslip, while the deeper megathrust did not. We interpret this temporarily increased shallow SSE recurrence rate to be driven by static stress loading from large afterslip.

Plain Language Summary Slow slip events (SSEs) are a type of fault movement that happens gradually, without causing earthquakes. Many of these events occur in subduction zones, where one tectonic plate subducts under another. While some SSEs are triggered by earthquake waves, it's rare to see them caused by slower fault slip process. In this study, we investigated the SSE phenomena at the Nicoya Peninsula in Costa Rica, where a magnitude 7.6 earthquake happened in 2012. We observed that shallow SSEs (typically within 20 km to the surface) happened more frequently in the first 1.5 years after that earthquake. These events occurred just next to the part of the fault that continued to slowly shift for months after the earthquake—a process known as afterslip. Deeper SSEs (typically occur at greater than 20 km depth), however, did not show this change. By modeling stress change on the fault, we found that the area with the increased SSE activity experienced an increase of stress due to the afterslip. We suggest that this extra stress temporarily caused shallow SSEs to occur more often, while deeper parts of the fault weren't affected in the same way.

1. Introduction

Slow slip events (SSEs) in subduction zones and other tectonic settings have been observed by various geodetic data in the last two decades (e.g., Araki et al., 2017; Bartlow et al., 2011; Brudzinski et al., 2016; Chen et al., 2018; Dragert et al., 2001; Jiang et al., 2012; Kato & Nakagawa, 2014; Michel et al., 2019; Obara et al., 2004; Ohta et al., 2006; Okada & Nishimura, 2023; Wallace et al., 2016). Some studies suggest that SSEs can trigger or evolve into large and great earthquakes (Obara & Kato, 2016; Segall & Bradley, 2012; Uchida et al., 2004, 2016); others suggest that SSEs may also limit the size or frequency of future earthquakes by relieving some of the accumulated stress and strain (e.g., Dixon et al., 2014). SSEs can occur independently or be triggered by stress changes resulting from earthquakes (Peng & Gomberg, 2010; Rolandone et al., 2018; Tymofyeyeva et al., 2019; Wallace et al., 2017). While some reported SSEs are triggered by dynamic stress changes, there are limited examples of SSEs caused by static-stress perturbations (Frank et al., 2016; Katakami et al., 2020; Miyazaki et al., 2006; Wallace et al., 2012, 2017). One such example occurred at a strike-slip fault after the 1987 M_w 6.6 Superstition Hills earthquake in southern California, where Wei et al. (2013) attributed the time-dependent changes in the intervals between creep events to loading rate changes and frictional heterogeneity. In this study, we report an increase in the shallow SSE recurrence rate in northwestern Costa Rica, where large stress perturbation occurred during afterslip from the 2012 M_w 7.6 megathrust earthquake.

SSEs in the Nicoya megathrust along the Middle America Trench have been documented since 2002 (Brown et al., 2005), and well recorded by a continuous GPS (cGPS) network since 2007 (Outerbridge et al., 2010; Figure 1a). On 5 September 2012, a M_w 7.6 earthquake struck the region (Davis et al., 2015; Protti et al., 2014;

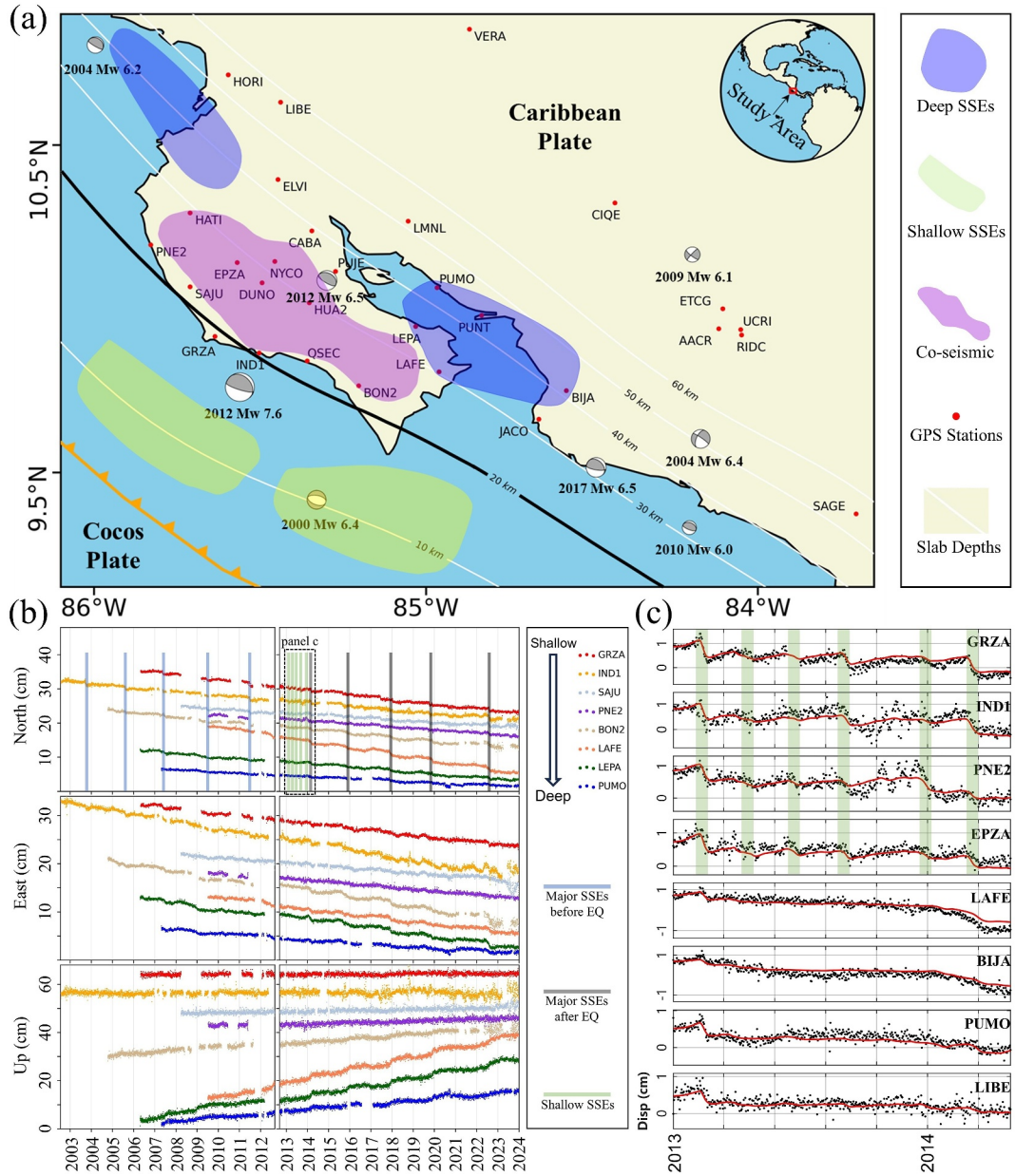

Figure 1. GPS data in the study region. (a) GPS network in northwestern Costa Rica. The red dots mark the locations of all available GPS stations in this study, with four-character station IDs labeled. The white contours mark the subduction plate interface depths from Slab2 model (Hayes et al., 2018). The beach balls indicate $M_w \geq 6$ earthquakes from 2000 to 2024 (Yue et al. (2013) and USGS catalog). The orange line shows the trench. The thick black line is the 20 km slab depth contour separating deep and shallow subducting portions. The light green and blue areas are the regions with shallow and deep inter-seismic slow slip events (SSEs), respectively (Dixon et al., 2014). The light purple area is the >1 m co-seismic rupture area due to the 2012 M_w 7.6 earthquake (Kyriakopoulos & Newman, 2016). (b) GPS displacement time series of the entire observational period for selected stations, arranged by slab depth from shallow to deep, with seasonal variations, co-seismic and post-seismic deformation, and inter-SSE trends removed. Displacements were offset arbitrarily for clarity. (c) Selected GPS displacement time series in the first 1.5 years following the 2012 M_w 7.6 earthquake, the dots and red lines show the observed and modeled time series of north component, respectively. The light green shaded areas mark the six detected shallow SSEs.

Yue et al., 2013). Co-seismic deformation occurred on a portion of the plate interface where a high ratio of late inter-seismic coupling (locking) was observed (Feng et al., 2012; Kyriakopoulos & Newman, 2016; Protti et al., 2014; Sun et al., 2017). Data acquired in the first 2 years following the earthquake revealed large afterslip on

part of the previously locked zone that did not rupture during the earthquake (Malservisi et al., 2015). Using land GPS and seafloor pressure records obtained within 1.3 years after the earthquake, Sun et al. (2017) demonstrated that the earthquake rupture did not reach the trench while the afterslip was trench-breaching. The cGPS data collected during the late and early stages of the earthquake cycle provide opportunities to study possible interactions between seismic and aseismic deformation. Previous studies suggest that the 2012 M_w 7.6 earthquake did not change the recurrence rate of large SSEs (equivalent to $M_w \geq 6.8$ earthquakes; which occurred in the deep portion of the megathrust, i.e., beneath the Gulf of Nicoya; Figure 1a; Voss et al., 2017; Xie et al., 2020). With more than 10 years of data now available after the 2012 M_w 7.6 earthquake, we re-examine this conclusion and report evidence of temporarily increased SSE recurrence rate in the shallow portion of the megathrust during the rapid afterslip stage.

2. Data Processing

Available data obtained by the cGPS network from July 2002 to January 2024 were analyzed following the framework of Xie et al. (2020). We first processed the GPS data into daily averaged positions with GipsyX v.2.3 (Bertiger et al., 2020). The position time series were then transformed into North/East/Up displacements relative to a priori site coordinates in the regional reference frame CARIB18 (Wang et al., 2019). We used the multichannel singular spectrum analysis to remove seasonal oscillation not associated with tectonic motion. Figure S1 in Supporting Information S1 shows example displacement time series with seasonal variations and inter-SSEs trends removed. To highlight SSEs, Figure 1b shows time series with (a) co-seismic displacements removed by step functions, (b) post-seismic deformation removed by exponential decay functions with characteristic times of 11, 94, 470, and 1,865 days, and (c) inter-SSE trends removed following Xie et al. (2020). Visual inspection of the time series and previous work (e.g., Xie et al., 2020) suggest that the recurrence interval of deep SSEs (indicated by reverse displacements observed at GPS stations over the deep plate interface) remains largely unchanged before and after the 2012 M_w 7.6 earthquake. However, several stations located above the shallowest plate interface under the Nicoya Peninsula, particularly GRZA, exhibit more frequent SSE-like displacements within 1.5 years after the earthquake (marked by the light green lines in Figure 1b and green shades in Figure 1c). The full set of data shown in Figure 1c is illustrated in Figure S2 in Supporting Information S1. GPS common mode error (CME), if significant, is difficult to eliminate due to the relatively small number of cGPS stations and complex tectonic signals in this region. However, CME should not alter the contrasting SSE behaviors between the shallow and deep portions because it will affect all stations across the region. In Nicoya, the average recurrence interval of major SSEs (mainly occurred in the deep portion) prior to the 2012 event is about 22 months, and the smaller and shallower SSEs occurred more irregularly, with typical recurrence intervals of 0.5–1 year. Within 1.5 years after the 2012 M_w 7.6 earthquake the recurrence interval of shallow SSEs became ∼2–3 months. After mid-2014, the recurrence interval of shallow SSEs resumed to its pre-earthquake level (with typical interval longer than 6 months). Below we use time-dependent inversion to investigate the SSE and afterslip characteristics from the GPS observed displacements.

3. Time-Dependent Slip Inversion

We applied a modified network inversion filter (NIF) to model the GPS displacements, summarized below (Bartlow et al., 2011; Liu et al., 2010, 2015; McGuire & Segall, 2003; Segall & Matthews, 1997). First, we created a triangular mesh to represent the plate interface from the trench to 60 km depth based on Slab 2.0 model (Fukushima et al., 2005; Hayes et al., 2018). The average length of element sides is ∼20 km. Second, we calculated the Green's function that relates fault slip to surface displacements in a homogeneous elastic half-space using the dislocation model of Jeyakumaran et al. (1992). Third, we solved for daily slip on individual fault elements in a regularized inversion. The inversion scheme is based on an extended Kalman filter, with non-negative slip constraint and temporal and spatial smoothing imposed. The preferred hyperparameters for temporal and spatial smoothing are based on maximum likelihood estimation and determined by the compromise between misfit and smoothness (Figure S3 in Supporting Information S1).

The time-dependent slip inversion reveals spatial and temporal variations of rapid afterslip, SSEs, and multiscale relaxation processes. Figure 2 shows cumulative slip and snapshots of slip rates from the inversion. During the modeled period multiple shallow SSEs occurred in the offshore region, whereas only one deep SSE occurred and it was immediately under the Gulf of Nicoya in early 2014. Figure S4 in Supporting Information S1 shows the observed and modeled GPS displacement time series of postseismic and SSEs for the first 3 years after the

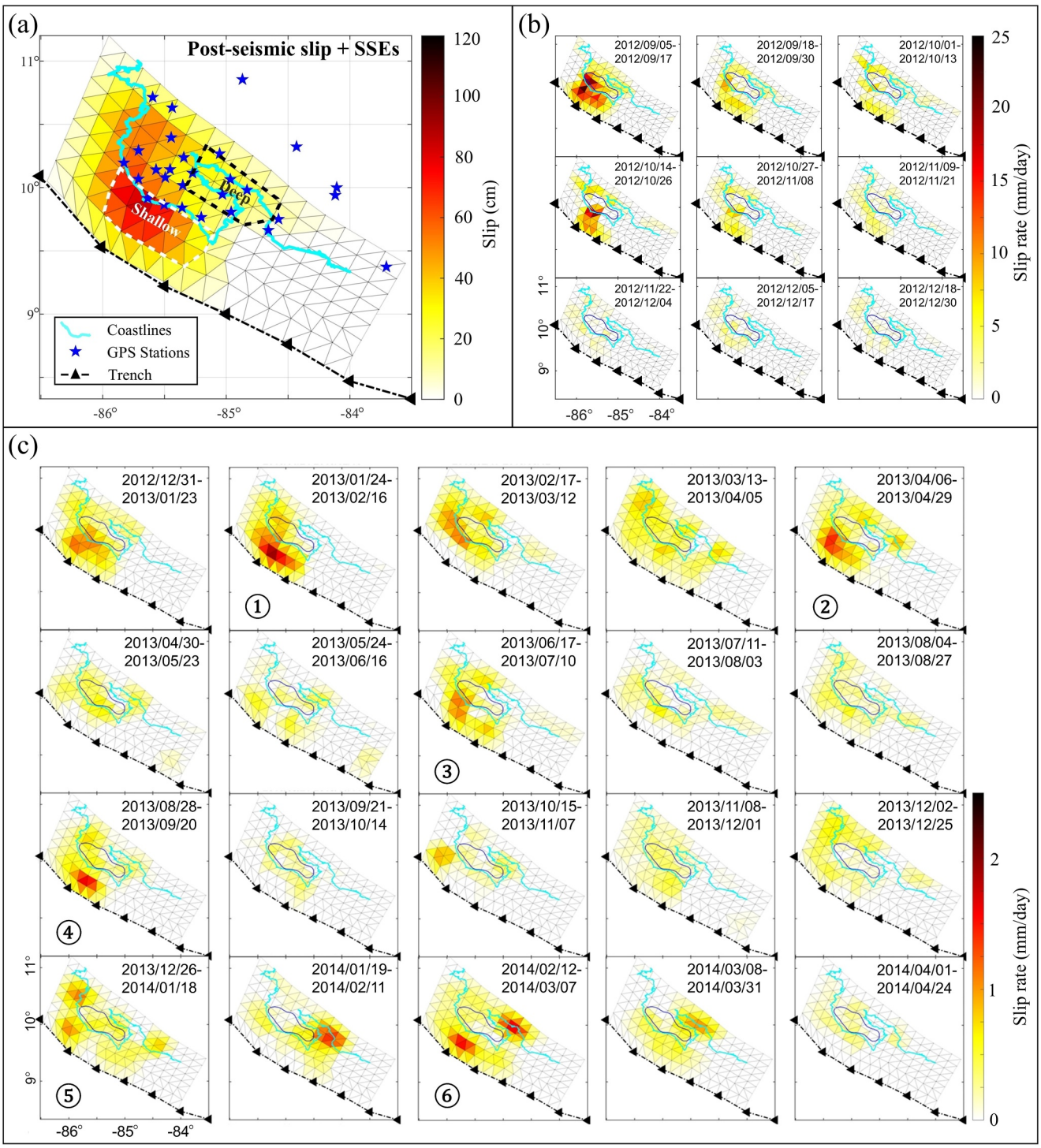

Figure 2. Time-dependent inversion of post-seismic slip and slow slip events (SSEs). (a) Accumulated post-seismic deformation and slow slip within 1,000 days after the 2012 M_w 7.6 earthquake. The dashed white and black polygons outline the shallow and deep portions where the moment release time series are shown in Figure 3. (b) Modeled rates of the afterslip within 4 months after the 2012 M_w 7.6 earthquake. (c) Modeled fault slip rates from January 2013 to April 2014 (the same period as Figure 1c). The observed shallow SSEs are highlighted by circled numbers 1–6 (corresponding to the light green shaded periods shown in Figure 1c).

earthquake. Apart from significant slip caused by the M_w 6.5 aftershock on 24 October 2012 (the map shown in the first column and second row of Figure 2b), large afterslip occurred immediately next to the co-seismic rupture zone in the first 2 weeks after the mainshock, and the slip rate decreased rapidly in the following weeks. Between

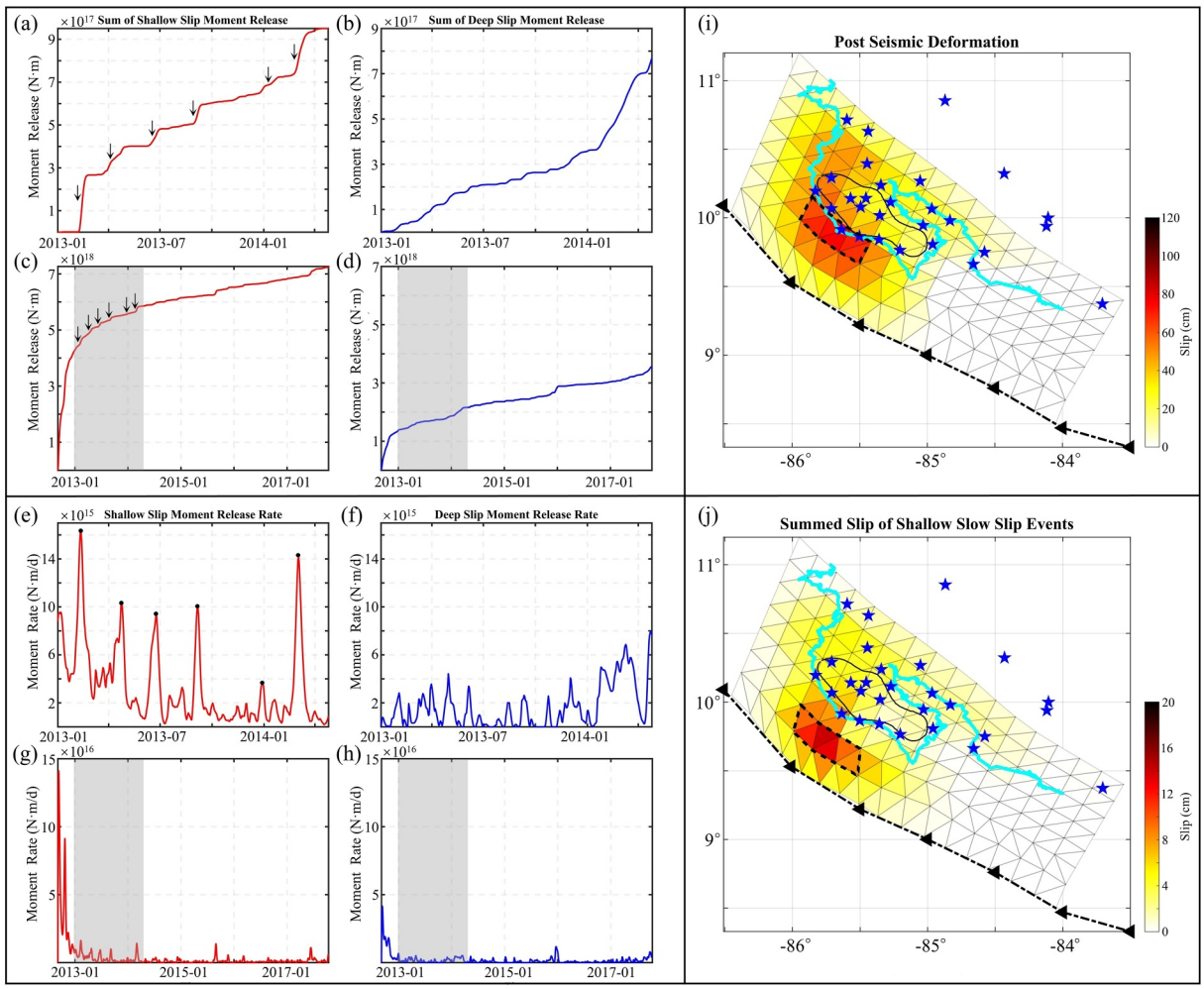

Figure 3. Time series of moment release for the shallow and deep portions of the subduction zone, with the respective areas outlined in Figure 2a. Data lengths in panels (a), (b), (e), and (f) correspond to the period within 1.5 years after the 2012 M_w 7.6 earthquake. Panels (c), (d), (g), (h) show the cumulative moment release and rate time series within 5 years after the 2012 M_w 7.6 earthquake. (a–d) Cumulative moment release in the shallow (panels a, c) and deep portions (panels b, d) of the subduction zone. The black arrows in (a) indicate the timing of shallow slow slip events (SSEs) identified in Figure 1c. (e–h) Moment release rates for the shallow (e, g) and deep (f, h) portions. The black dots in (e) mark the timing of shallow SSEs. In the longer time series plots (c, d, g, h), the gray shaded region highlights the time period corresponding to the period with increased shallow SSE frequency. (i) Accumulated post-seismic slip within 1.5 years following the 2012 M_w 7.6 earthquake. (j) Accumulated shallow slow slip within 1.5 years following the 2012 M_w 7.6 earthquake. The dashed black polygons in panels (i) and (j) outline the peak slip areas. The solid black lined shape indicates the >1 m co-seismic rupture area (Kyriakopoulos & Newman, 2016).

February 2013 and March 2014, six SSEs occurred in the shallow portion of the subduction plate interface, immediately adjacent to the area where large afterslip occurred (Figure 2c).

4. Results and Discussion

4.1. Temporarily Increased SSE Frequency After Significant Afterslip

A number of shallow SSEs before the 2012 M_w 7.6 earthquake were identified from land cGPS observations in the study region (e.g., Dixon et al., 2014). While there is evidence from ocean bottom pressure measurements at a CORK site that multiple SSEs occurred at the trench within the first month after the 2012 M_w 7.6 earthquake, displacements associated with those events at the land cGPS stations are small (Sun et al., 2017). With longer observations, our analysis suggests that frequent shallow SSEs with detectable surface displacements at some land cGPS stations occurred in the first 1.5 years after the 2012 earthquake. Further analysis of the moment release indicates that these shallow SSEs correspond to the period when the shallow portion has released significant amount of energy (Figures 2 and 3).

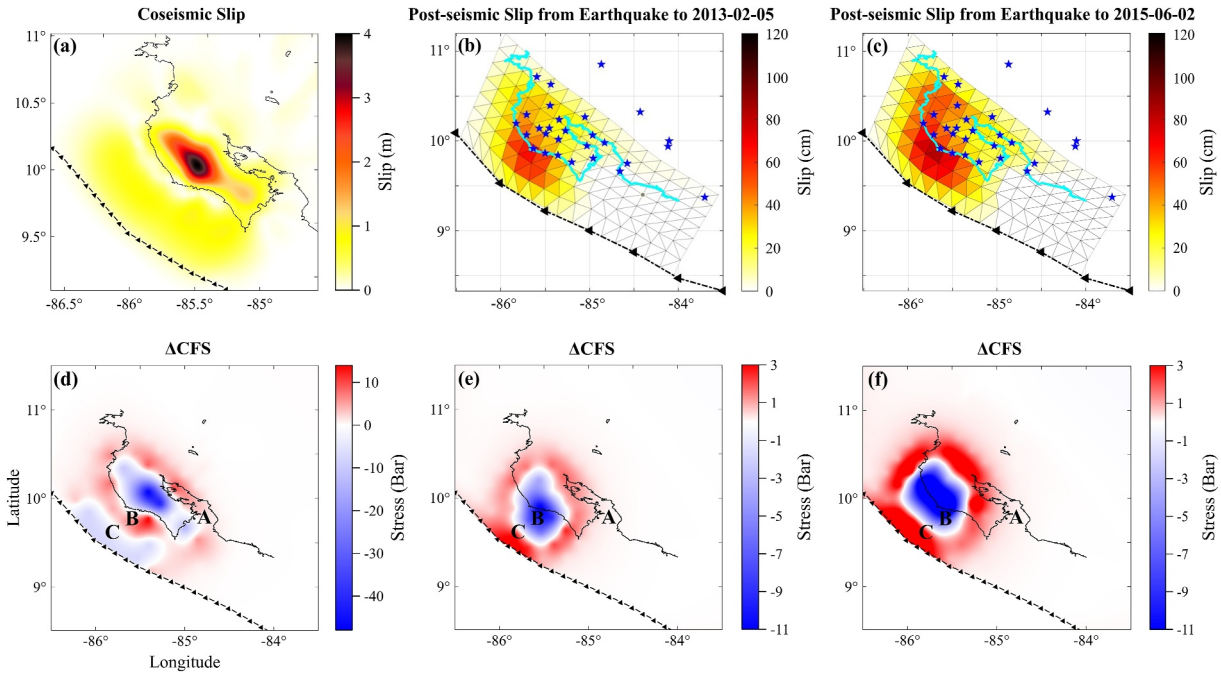

Figure 4. Co-seismic rupture and slip due to post-seismic and slow slip events (SSEs), and corresponding Coulomb stress changes. (a) The co-seismic slip of the 2012 M_w 7.6 earthquake (Kyriakopoulos & Newman, 2016). (b) Accumulated post-seismic slip between the 2012 M_w 7.6 earthquake and the first shallow SSE observed by land cGPS. (c) Accumulated post-seismic plus slow slip within 1,000 days after the 2012 M_w 7.6 earthquake. (d) Coulomb stress change caused by the co-seismic rupture of the 2012 M_w 7.6 earthquake. (e) Coulomb stress change caused by the slip shown in panel (b). (f) Coulomb stress change caused by the slip shown in panel (c). In panels (d–f), A labels the deep portion, B labels the portion with large afterslip, C labels the shallow portion immediately updip of the large afterslip zone.

The first column of Figure 3 illustrates the cumulative moment release (panels a, c) and the daily moment rate (panels e, g) time series during selected periods for the shallow portion outlined by the dashed white polygon in Figure 2a. Panels a and e show the results of shallow SSEs only, and panels c and g show the results due to post-seismic deformation plus SSEs. Note that panels a–h have different time spans, and the shorter periods shown in panels a, b, e, f are indicated by the shaded gray areas in panels c, d, g, h. In comparison, panels a and e show the occurrence of shallow SSEs, while panels c and g demonstrate the energy release due to the long-lasting post-seismic deformation. Comparative time series of the deep portion (outlined by the dashed black polygon in Figure 2a) are illustrated in the second column of Figure 3. For the shallow portion, multiple transient increases in the moment release rates correspond to the identified SSEs. For the deep portion, only one significant moment release event was observed in the first 1.5 years after the 2012 M_w 7.6 earthquake (it corresponds to columns 2–4 in the last row of Figure 2c). Within 5 years after the 2012 M_w 7.6 earthquake, the cumulative moment release time series exhibit a logarithmic decay plus multiple transient moment release events. Apart from long-lasting viscoelastic relaxation, the moment release rate decreased to nearly the background level in 2 years after the earthquake.

Figure 3i shows the cumulative afterslip within 1.5 years from the 2012 earthquake. Figure 3j shows the total slip due to shallow SSEs (sum of the highlighted events 1–6 in Figure 2c), outlining the primary SSE area. Resolution tests conducted in previous studies suggest that the land cGPS network can resolve fault slip for the nearshore region, within 30 km of the coast, but has poor resolution near the trench (e.g., Jiang et al., 2017; Kyriakopoulos & Newman, 2016; Xie et al., 2020). We conducted checkerboard resolution tests to examine the offshore resolution. The results demonstrate that the land cGPS network can resolve slip near the up-dip edge of the main afterslip zone at 25 km or lower resolution (Figures S5 and S6 in Supporting Information S1). With relatively high confidence, the afterslip is most significant near the coastline, that is, near the updip edge of the main co-seismic rupture (Figures 2–4). Shallow SSEs occur updip of the main afterslip zone, with the peak slip area lying between the trench and the peak afterslip zone (Figure 3j). Whether the shallow SSE area extend to the trench cannot be uniquely resolved with available land GPS data.

4.2. The Role of Stress Loading Increase Driven by Afterslip

Crustal deformation is directly associated with stress and strain conditions. To better understand the observation that more frequent shallow SSEs occurred in the vicinity of the large afterslip zone shortly after the 2012 M_w 7.6 earthquake, we employed the widely used Coulomb Failure Stress change (ΔCFS) model to probe stress conditions on the plate interface during and after the 2012 earthquake. The ΔCFS model looks at how the ratio of normal to shear stress on a particular fault surface changes as a result of an earthquake, afterslip, or other major stress perturbation. Positive ΔCFS is interpreted to promote failure, while negative ΔCFS inhibits failure (e.g., King et al., 1994; Lin & Stein, 2004; Stein et al., 1992; Voss et al., 2018). Figure 4d shows ΔCFS caused by the co-seismic deformation. As expected, large positive changes in ΔCFS are observed surrounding the co-seismic rupture zone. However, subsequent fault behavior depends on location and pre-earthquake SSE activity.

In area A (annotated in Figures 4d–4f), while the earthquake rupture caused a positive ΔCFS, afterslip here was trivial. This likely reflects lack of significant pre-earthquake strain accumulation here because, large SSEs occur approximately every 22 months, releasing nearly all accumulated strain (Dixon et al., 2014; Xie et al., 2020). Hence, the recurrence interval of the deep SSE patch does not change.

Area B was previously identified to be a nearly fully locked patch (i.e., with large slip deficit) late in the earthquake cycle but did not rupture during the 2012 M_w 7.6 earthquake (e.g., Feng et al., 2012; Protti et al., 2014). The large increase in stress loading caused by the co-seismic rupture, as evident in the ΔCFS map shown in Figure 4d, likely promoted afterslip here. Panels b and e in Figure 4 illustrate the cumulative afterslip and stress change from the earthquake to the beginning of the first observed shallow SSE.

Previous studies suggest that an increase of ∼3 bar in ΔCFS is sufficiently large to influence the genesis of episodic slip events (e.g., Rubinstein et al., 2008; Wallace et al., 2017). The pre-strained area C reached this level shortly after the M_w 7.6 earthquake due to large afterslip (Figure 4e). By mid-2014, the strain was mostly released, and the shallow SSE frequency returned to the pre-earthquake level.

Variations in pore pressure and frictional properties between shallow and deep megathrust segments may influence how sensitive SSEs are to stress perturbations. The shallow interface, typically exhibiting high pore pressure from sediment compaction and dehydration (Saffer & Tobin, 2011), may be more prone to SSEs triggered by stress changes, as supported by numerical models (Dong et al., 2022; Heimisson et al., 2019; Perez-Silva et al., 2023). Modeling results suggest that poroelastic deformation contributed significantly to early postseismic surface motion beneath the Nicoya Peninsula and trenchward (shallow region), but had minimal impact beneath the Gulf of Nicoya, likely due to differences in permeability and fluid pressure gradients (McCormack et al., 2020).

The shallow portion of many subduction zones is characterized by conditionally stable friction and can be highly sensitive to small stress changes. For instance, with seismic data, Frank et al. (2016) found that stress changes of just a few kPa can influence shallow seismicity in the Guerrero segment of the Mexican subduction zone. While offshore geodetic observations are scarce, the proximity of the trench to land in Nicoya allows coastal GPS stations to record shallow SSEs. With the development of seafloor geodetic instrumentation in subduction zones, phenomena similar to the discussed example may be observed in other places.

5. Conclusions

Long-duration continuous GPS data collected across the 2012 M_w 7.6 earthquake in Nicoya Peninsula suggest a temporarily increased recurrence rate of shallow SSEs in the early stage of post-seismic deformation. Our time-dependent modeling of fault slip and Coulomb stress changes indicates that the slow slip area is in the immediate proximity of the area with significant Coulomb stress increase. The good correlation between the timing of more frequent shallow SSEs and significant cumulative afterslip is strong evidence that stress loading driven by afterslip promotes the occurrence of shallow SSEs in the Nicoya megathrust.

Data Availability Statement

Raw data collected at CIQE, CIQU, LIBE, NICY, NYCO, PUNT, RIDC, and SAGE stations can be found from the Instituto Geográfico Nacional website (https://gnss.rnp.go.cr/SBC/). Daily position time series of ETCG,

UCRI, and AACR stations were provided by the Nevada Geodetic Laboratory (Blewitt et al., 2018). Daily position time series of station DUNO, HORI, and JACO stations are available from Xie (2025). Rinex observational files for all the other GPS stations used in this paper are archived at the EarthScope repository, including: GRZA (Dixon & Protti, 2006a), IND1 (Dixon & Protti, 2010b), SAJU (Dixon & Protti, 2008a), PNE2 (Dixon & Protti, 2010c), PNEG (Dixon & Protti, 2009a), QSEC (Dixon & Protti, 2006b), BON2 (Dixon & Protti, 2009b), EPZA (Dixon & Protti, 2009c), HATI (Dixon & Protti, 2007a), HUA2 (Dixon & Protti, 2009d), LAFE (Dixon & Protti, 2009e), LEPA (Dixon & Protti, 2006c), PUJE (Dixon & Protti, 2009f), CABA (Dixon & Protti, 2010d), BIJA (Dixon & Protti, 2010a), PUMO (Dixon & Protti, 2008b), ELVI (Dixon & Protti, 2008c), LMNL (Dixon & Protti, 2007b), and VERA (Dixon & Protti, 2010e).

Acknowledgments

This research was supported by National Science Foundation Grant 2314272 to SX and by the Universidad Nacional de Costa Rica through project PPAA 0426-24 to MP and project 0097-2020 to CM. Most of the stations reported here are jointly operated by OVSICORI-UNA and EarthScope Consortium, and we thank personnel at these institutions for network maintenance. The authors would like to acknowledge Álvaro A. Álvarez Calderón from the Instituto Geografico Nacional (IGN; https://gnss.rnp.go.cr/SBC/) for his work in collecting and providing GNSS data from stations they operate. Timothy Dixon at the University of South Florida is thanked for his comments on an earlier version of the manuscript. We are grateful to Noel Jackson at the University of Kansas for maintaining the NIF software and offering valuable technical support. We thank JPL/NASA for providing the GipsyX software for GPS data processing. Laura Wallace and an anonymous reviewer are acknowledged for their constructive comments. Gratitude is expressed to editor Christian Huber for his help with the technical issue encountered during the submission of the revision.

References

Araki, E., Saffer, D. M., Kopf, A. J., Wallace, L. M., Kimura, T., Machida, Y., et al. (2017). Recurring and triggered slow-slip events near the trench at the Nankai Trough subduction megathrust. *Science*, *356*(6343), 1157–1160. https://doi.org/10.1126/science.aan3120

Bartlow, N. M., Miyazaki, S. I., Bradley, A. M., & Segall, P. (2011). Space-time correlation of slip and tremor during the 2009 Cascadia slow slip event. *Geophysical Research Letters*, *38*(18), L18309. https://doi.org/10.1029/2011GL048714

Bertiger, W., Bar-Sever, Y., Dorsey, A., Haines, B., Harvey, N., Hemberger, D., et al. (2020). GipsyX/RTGx, a new tool set for space geodetic operations and research. *Advances in Space Research*, *66*(3), 469–489. https://doi.org/10.1016/j.asr.2020.04.015

Blewitt, G., Hammond, W. C., & Kreemer, C. (2018). Harnessing the GPS data explosion for interdisciplinary science. *Eos*, *99*, e2020943118. https://doi.org/10.1029/2018EO104623

Brown, K. M., Tryon, M. D., DeShon, H. R., Dorman, L. M., & Schwartz, S. Y. (2005). Correlated transient fluid pulsing and seismic tremor in the Costa Rica subduction zone. *Earth and Planetary Science Letters*, *238*(1–2), 189–203. https://doi.org/10.1016/j.epsl.2005.06.055

Brudzinski, M. R., Schlanser, K. M., Kelly, N. J., DeMets, C., Grand, S. P., Márquez-Azúa, B., & Cabral-Cano, E. (2016). Tectonic tremor and slow slip along the northwestern section of the Mexico subduction zone. *Earth and Planetary Science Letters*, *454*, 259–271. https://doi.org/10.1016/j.epsl.2016.08.004

Chen, S. K., Wu, Y. M., & Chan, Y. C. (2018). Episodic slow slip events and overlying plate seismicity at the southernmost Ryukyu Trench. *Geophysical Research Letters*, *45*(19), 10–369. https://doi.org/10.1029/2018GL079740

Davis, E. E., Villinger, H., & Sun, T. (2015). Slow and delayed deformation and uplift of the outermost subduction prism following ETS and seismogenic slip events beneath Nicoya Peninsula, Costa Rica. *Earth and Planetary Science Letters*, *410*, 117–127. https://doi.org/10.1016/j.epsl.2014.11.015

Dixon, T. H., Jiang, Y., Malservisi, R., McCaffrey, R., Voss, N., Protti, M., & Gonzalez, V. (2014). Earthquake and tsunami forecasts: Relation of slow slip events to subsequent earthquake rupture. *Proceedings of the National Academy of Sciences*, *111*(48), 17039–17044. https://doi.org/10.1073/pnas.1412299111

Dixon, T. H., & Protti, M. (2006a). Costa Rica GPS network—GRZA-Garza P.S., the NSF GAGE Facility operated by EarthScope Consortium [Dataset]. *GPS/GNSS Observations*. https://doi.org/10.7283/T5HX19V3

Dixon, T. H., & Protti, M. (2006b). Costa Rica GPS network—QSEC-Quebrada Seca P.S., the NSF GAGE Facility operated by EarthScope Consortium [Dataset]. *GPS/GNSS Observations*. https://doi.org/10.7283/T5SF2TBM

Dixon, T. H., & Protti, M. (2006c). Costa Rica GPS network—LEPA-Lepanto P.S., the NSF GAGE Facility operated by EarthScope Consortium [Dataset]. *GPS/GNSS Observations*. https://doi.org/10.7283/T5NP22M8

Dixon, T. H., & Protti, M. (2007a). Costa Rica GPS network—HATI-Hatillo P.S., the NSF GAGE Facility operated by EarthScope Consortium [Dataset]. *GPS/GNSS Observations*. https://doi.org/10.7283/T5X34VM5

Dixon, T. H., & Protti, M. (2007b). Costa Rica GPS network—LMNL-Limonal P.S., the NSF GAGE Facility operated by EarthScope Consortium [Dataset]. *GPS/GNSS Observations*. https://doi.org/10.7283/T51V5C3J

Dixon, T. H., & Protti, M. (2008a). Costa Rica GPS network—SAJU-Puerto San Juanillo P.S., the NSF GAGE Facility operated by EarthScope Consortium [Dataset]. *GPS/GNSS Observations*. https://doi.org/10.7283/T5F47M9C

Dixon, T. H., & Protti, M. (2008b). Costa Rica GPS network—PUMO-Punto Morales P.S., the NSF GAGE Facility operated by EarthScope Consortium [Dataset]. *GPS/GNSS Observations*. https://doi.org/10.7283/T55M63V9

Dixon, T. H., & Protti, M. (2008c). Costa Rica GPS network—ELVI-El Viejo P.S., the NSF GAGE Facility operated by EarthScope Consortium [Dataset]. *GPS/GNSS Observations*. https://doi.org/10.7283/T59C6VKN

Dixon, T. H., & Protti, M. (2009a). Costa Rica GPS network—PNEG-Playa Negra P.S., the NSF GAGE Facility operated by EarthScope Consortium [Dataset]. *GPS/GNSS Observations*. https://doi.org/10.7283/T50V89ZR

Dixon, T. H., & Protti, M. (2009b). Costa Rica GPS network—BON2-Bongo P.S., the NSF GAGE Facility operated by EarthScope Consortium [Dataset]. *GPS/GNSS Observations*. https://doi.org/10.7283/T5W66HXJ

Dixon, T. H., & Protti, M. (2009c). Costa Rica GPS network—EPZA-Esperanza P.S., the NSF GAGE Facility operated by EarthScope Consortium [Dataset]. *GPS/GNSS Observations*. https://doi.org/10.7283/T5JW8C1S

Dixon, T. H., & Protti, M. (2009d). Costa Rica GPS network—HUA2-Huacas P.S., the NSF GAGE Facility operated by EarthScope Consortium [Dataset]. *GPS/GNSS Observations*. https://doi.org/10.7283/T5RF5S67

Dixon, T. H., & Protti, M. (2009e). Costa Rica GPS network—LAFE-Finca La Fe P.S., the NSF GAGE Facility operated by EarthScope Consortium [Dataset]. *GPS/GNSS Observations*. https://doi.org/10.7283/T57D2S80

Dixon, T. H., & Protti, M. (2009f). Costa Rica GPS network— PUJE-Puerto Jesus P.S., the NSF GAGE Facility operated by EarthScope Consortium [Dataset]. *GPS/GNSS Observations*. https://doi.org/10.7283/T54M92PG

Dixon, T. H., & Protti, M. (2010a). Costa Rica GPS network—BIJA-Bijagual P.S., the NSF GAGE Facility operated by EarthScope Consortium [Dataset]. *GPS/GNSS Observations*. https://doi.org/10.7283/T5C53J0Q

Dixon, T. H., & Protti, M. (2010b). Costa Rica GPS network—IND1-Punta Indio P.S., the NSF GAGE Facility operated by EarthScope Consortium [Dataset]. *GPS/GNSS Observations*. https://doi.org/10.7283/T58C9TDT

Dixon, T. H., & Protti, M. (2010c). Costa Rica GPS network—PNE2-Playa Negra 2 P.S., the NSF GAGE Facility operated by EarthScope Consortium [Dataset]. *GPS/GNSS Observations*. https://doi.org/10.7283/T5D50K43

Dixon, T. H., & Protti, M. (2010d). Costa Rica GPS network—CABA-Caballito P.S., the NSF GAGE Facility operated by EarthScope Consortium [Dataset]. *GPS/GNSS Observations*. https://doi.org/10.7283/T5GX48QQ

Dixon, T. H., & Protti, M. (2010e). Costa Rica GPS network—VERA-Veracruz P.S., the NSF GAGE Facility operated by EarthScope Consortium [Dataset]. *GPS/GNSS Observations*. https://doi.org/10.7283/T5MP51FF

Dong, P., Xu, R., Yang, H., Guo, Z., & Xia, K. (2022). Fault slip behaviors modulated by locally increased fluid pressure: Earthquake nucleation and slow slip events. *Journal of Geophysical Research: Solid Earth*, *127*(12), e2022JB024612. https://doi.org/10.1029/2022JB024612

Dragert, H., Wang, K., & James, T. S. (2001). A silent slip event on the deeper Cascadia subduction interface. *Science*, *292*(5521), 1525–1528. https://doi.org/10.1126/science.1060152

Feng, L., Newman, A. V., Protti, M., González, V., Jiang, Y., & Dixon, T. H. (2012). Active deformation near the Nicoya Peninsula, northwestern Costa Rica, between 1996 and 2010: Interseismic megathrust coupling. *Journal of Geophysical Research*, *117*(B6). https://doi.org/10.1029/2012JB009230

Frank, W. B., Shapiro, N. M., Husker, A. L., Kostoglodov, V., & Campillo, M. (2016). Repeating seismicity in the shallow crust modulated by transient stress perturbations. *Tectonophysics*, *687*, 105–110. https://doi.org/10.1016/j.tecto.2016.09.003

Fukushima, Y., Cayol, V., & Durand, P. (2005). Finding realistic dike models from interferometric synthetic aperture radar data: The February 2000 eruption at Piton de la Fournaise. *Journal of Geophysical Research*, *110*(B3). https://doi.org/10.1029/2004jb003268

Hayes, G. P., Moore, G. L., Portner, D. E., Hearne, M., Flamme, H., Furtney, M., & Smoczyk, G. M. (2018). Slab2, a comprehensive subduction zone geometry model. *Science*, *362*(6410), 58–61. https://doi.org/10.1126/science.aat4723

Heimisson, E. R., Dunham, E. M., & Almquist, M. (2019). Poroelastic effects destabilize mildly rate-strengthening friction to generate stable slow slip pulses. *Journal of the Mechanics and Physics of Solids*, *130*, 262–279. https://doi.org/10.1016/j.jmps.2019.06.007

Jeyakumaran, M., Rudnicki, J. W., & Keer, L. M. (1992). Modeling slip zones with triangular dislocation elements. *Bulletin of the Seismological Society of America*, *82*(5), 2153–2169. https://doi.org/10.1785/BSSA0820052153

Jiang, Y., Liu, Z., Davis, E. E., Schwartz, S. Y., Dixon, T. H., Voss, N., et al. (2017). Strain release at the trench during shallow slow slip: The example of Nicoya Peninsula, Costa Rica. *Geophysical Research Letters*, *44*(10), 4846–4854. https://doi.org/10.1002/2017GL072803

Jiang, Y., Wdowinski, S., Dixon, T. H., Hackl, M., Protti, M., & Gonzalez, V. (2012). Slow slip events in Costa Rica detected by continuous GPS observations, 2002–2011. *Geochemistry, Geophysics, Geosystems*, *13*(4), 4006. https://doi.org/10.1029/2012GC004058

Katakami, S., Kaneko, Y., Ito, Y., & Araki, E. (2020). Stress sensitivity of instantaneous dynamic triggering of shallow slow slip events. *Journal of Geophysical Research: Solid Earth*, *125*(6), e2019JB019178. https://doi.org/10.1029/2019JB019178

Kato, A., & Nakagawa, S. (2014). Multiple slow-slip events during a foreshock sequence of the 2014 Iquique, Chile Mw 8.1 earthquake. *Geophysical Research Letters*, *41*(15), 5420–5427. https://doi.org/10.1002/2014GL061138

King, G. C., Stein, R. S., & Lin, J. (1994). Static stress changes and the triggering of earthquakes. *Bulletin of the Seismological Society of America*, *84*(3), 935–953. https://doi.org/10.1785/BSSA0840030935

Kyriakopoulos, C., & Newman, A. V. (2016). Structural asperity focusing locking and earthquake slip along the Nicoya megathrust, Costa Rica. *Journal of Geophysical Research: Solid Earth*, *121*(7), 5461–5476. https://doi.org/10.1002/2016JB012886

Lin, J., & Stein, R. S. (2004). Stress triggering in thrust and subduction earthquakes and stress interaction between the southern San Andreas and nearby thrust and strike-slip faults. *Journal of Geophysical Research*, *109*(B2), 19. https://doi.org/10.1029/2003JB002607

Liu, Z., Moore, A. W., & Owen, S. (2015). Recurrent slow slip event reveals the interaction with seismic slow earthquakes and disruption from large earthquake. *Geophysical Journal International*, *202*(3), 1555–1565. https://doi.org/10.1093/gji/ggv238

Liu, Z., Owen, S., Dong, D., Lundgren, P., Webb, F., Hetland, E., & Simons, M. (2010). Integration of transient strain events with models of plate coupling and areas of great earthquakes in southwest Japan. *Geophysical Journal International*, *181*(3), 1292–1312. https://doi.org/10.1111/j.1365-246X.2010.04599.x

Malservisi, R., Schwartz, S. Y., Voss, N., Protti, M., Gonzalez, V., Dixon, T. H., et al. (2015). Multiscale postseismic behavior on a megathrust: The 2012 Nicoya earthquake, Costa Rica. *Geochemistry, Geophysics, Geosystems*, *16*(6), 1848–1864. https://doi.org/10.1002/2015GC005794

McCormack, K., Hesse, M. A., Dixon, T., & Malservisi, R. (2020). Modeling the contribution of poroelastic deformation to postseismic geodetic signals. *Geophysical Research Letters*, *47*(8), e2020GL086945. https://doi.org/10.1029/2020GL086945

McGuire, J. J., & Segall, P. (2003). Imaging of aseismic fault slip transients recorded by dense geodetic networks. *Geophysical Journal International*, *155*(3), 778–788. https://doi.org/10.1111/j.1365-246X.2003.02022.x

Michel, S., Gualandi, A., & Avouac, J. P. (2019). Similar scaling laws for earthquakes and Cascadia slow-slip events. *Nature*, *574*(7779), 522–526. https://doi.org/10.1038/s41586-019-1673-6

Miyazaki, S. I., Segall, P., McGuire, J. J., Kato, T., & Hatanaka, Y. (2006). Spatial and temporal evolution of stress and slip rate during the 2000 Tokai slow earthquake. *Journal of Geophysical Research*, *111*(B3), B03409. https://doi.org/10.1029/2004JB003426

Obara, K., Hirose, H., Yamamizu, F., & Kasahara, K. (2004). Episodic slow slip events accompanied by non-volcanic tremors in southwest Japan subduction zone. *Geophysical Research Letters*, *31*(23), L23602. https://doi.org/10.1029/2004GL020848

Obara, K., & Kato, A. (2016). Connecting slow earthquakes to huge earthquakes. *Science*, *353*(6296), 253–257. https://doi.org/10.1126/science.aaf1512

Ohta, Y., Freymueller, J. T., Hreinsdóttir, S., & Suito, H. (2006). A large slow slip event and the depth of the seismogenic zone in the south central Alaska subduction zone. *Earth and Planetary Science Letters*, *247*(1–2), 108–116. https://doi.org/10.1016/j.epsl.2006.05.013

Okada, Y., & Nishimura, T. (2023). Systematic detection of short-term slow slip events in Southcentral Alaska. *Geophysical Research Letters*, *50*(17), e2023GL104901. https://doi.org/10.1029/2023GL104901

Outerbridge, K. C., Dixon, T. H., Schwartz, S. Y., Walter, J. I., Protti, M., Gonzalez, V., et al. (2010). A tremor and slip event on the Cocos-Caribbean subduction zone as measured by a global positioning system (GPS) and seismic network on the Nicoya Peninsula, Costa Rica. *Journal of Geophysical Research: Solid Earth*, *115*(B10), B10408. https://doi.org/10.1029/2009JB006845

Peng, Z., & Gomberg, J. (2010). An integrated perspective of the continuum between earthquakes and slow-slip phenomena. *Nature Geoscience*, *3*(9), 599–607. https://doi.org/10.1038/ngeo940

Perez-Silva, A., Kaneko, Y., Savage, M., Wallace, L., & Warren-Smith, E. (2023). Characteristics of slow slip events Explained by rate-strengthening faults Subject to periodic pore fluid pressure changes. *Journal of Geophysical Research: Solid Earth*, *128*(6), e2022JB026332. https://doi.org/10.1029/2022JB026332

Protti, M., González, V., Newman, A. V., Dixon, T. H., Schwartz, S. Y., Marshall, J. S., et al. (2014). Nicoya earthquake rupture anticipated by geodetic measurement of the locked plate interface. *Nature Geoscience*, *7*(2), 117–121. https://doi.org/10.1038/ngeo2038

Rolandone, F., Nocquet, J. M., Mothes, P. A., Jarrin, P., Vallée, M., Cubas, N., et al. (2018). Areas prone to slow slip events impede earthquake rupture propagation and promote afterslip. *Science Advances*, *4*(1), eaao6596. https://doi.org/10.1126/sciadv.aao6596

Rubinstein, J. L., La Rocca, M., Vidale, J. E., Creager, K. C., & Wech, A. G. (2008). Tidal modulation of nonvolcanic tremor. *Science*, *319*(5860), 186–189. https://doi.org/10.1126/science.1150558

Saffer, D. M., & Tobin, H. J. (2011). Hydrogeology and mechanics of subduction zone forearcs: Fluid flow and pore pressure. *Annual Review of Earth and Planetary Sciences*, *39*(1), 157–186. https://doi.org/10.1146/annurev-earth-040610-133408

Segall, P., & Bradley, A. M. (2012). Slow-slip evolves into megathrust earthquakes in 2D numerical simulations. *Geophysical Research Letters*, *39*(18), L18308. https://doi.org/10.1029/2012GL052811

Segall, P., & Matthews, M. (1997). Time dependent inversion of geodetic data. *Journal of Geophysical Research*, *102*(B10), 22391–22409. https://doi.org/10.1029/97JB01795

Stein, R. S., King, G. C., & Lin, J. (1992). Change in failure stress on the southern San Andreas fault system caused by the 1992 magnitude= 7.4 Landers earthquake. *Science*, *258*(5086), 1328–1332. https://doi.org/10.1126/science.258.5086.1328

Sun, T., Davis, E. E., Wang, K., & Jiang, Y. (2017). Trench-breaching afterslip following deeper coseismic slip of the 2012 Mw 7.6 Costa Rica earthquake constrained by near-trench pressure and land-based geodetic observations. *Earth and Planetary Science Letters*, *479*, 263–272. https://doi.org/10.1016/j.epsl.2017.09.021

Tymofyeyeva, E., Fialko, Y., Jiang, J., Xu, X., Sandwell, D., Bilham, R., et al. (2019). Slow slip event on the Southern San Andreas Fault triggered by the 2017 Mw 8.2 Chiapas (Mexico) earthquake. *Journal of Geophysical Research: Solid Earth*, *124*(9), 9956–9975. https://doi.org/10.1029/2018JB016765

Uchida, N., Hasegawa, A., Matsuzawa, T., & Igarashi, T. (2004). Pre-and post-seismic slow slip on the plate boundary off Sanriku, NE Japan associated with three interplate earthquakes as estimated from small repeating earthquake data. *Tectonophysics*, *385*(1–4), 1–15. https://doi.org/10.1016/j.tecto.2004.04.015

Uchida, N., Iinuma, T., Nadeau, R. M., Bürgmann, R., & Hino, R. (2016). Periodic slow slip triggers megathrust zone earthquakes in northeastern Japan. *Science*, *351*(6272), 488–492. https://doi.org/10.1126/science.aad3108

Voss, N., Dixon, T. H., Liu, Z., Malservisi, R., Protti, M., & Schwartz, S. (2018). Do slow slip events trigger large and great megathrust earthquakes? *Science Advances*, *4*(10), eaat8472. https://doi.org/10.1126/sciadv.aat8472

Voss, N. K., Malservisi, R., Dixon, T. H., & Protti, M. (2017). Slow slip events in the early part of the earthquake cycle. *Journal of Geophysical Research: Solid Earth*, *122*(8), 6773–6786. https://doi.org/10.1002/2016JB013741

Wallace, L. M., Beavan, J., Bannister, S., & Williams, C. (2012). Simultaneous long-term and short-term slow slip events at the Hikurangi subduction margin, New Zealand: Implications for processes that control slow slip event occurrence, duration, and migration. *Journal of Geophysical Research*, *117*(B11), 17–34. https://doi.org/10.1029/2012JB009489

Wallace, L. M., Kaneko, Y., Hreinsdóttir, S., Hamling, I., Peng, Z., Bartlow, N., et al. (2017). Large-scale dynamic triggering of shallow slow slip enhanced by overlying sedimentary wedge. *Nature Geoscience*, *10*(10), 765–770. https://doi.org/10.1038/ngeo3021

Wallace, L. M., Webb, S. C., Ito, Y., Mochizuki, K., Hino, R., Henrys, S., et al. (2016). Slow slip near the trench at the Hikurangi subduction zone, New Zealand. *Science*, *352*(6286), 701–704. https://doi.org/10.1126/science.aaf2349

Wang, G., Liu, H., Mattioli, G. S., Miller, M. M., Feaux, K., & Braun, J. (2019). CARIB18: A stable geodetic reference frame for geological hazard monitoring in the Caribbean region. *Remote Sensing*, *11*(6), 680. https://doi.org/10.3390/rs11060680

Wei, M., Kaneko, Y., Liu, Y., & McGuire, J. J. (2013). Episodic fault creep events in California controlled by shallow frictional heterogeneity. *Nature Geoscience*, *6*(7), 566–570. https://doi.org/10.1038/ngeo1835

Xie, S. (2025). Daily position time series of the continuous GPS network in Nicoya Peninsula, Costa Rica. *Zenodo*. https://doi.org/10.5281/zenodo.15686553

Xie, S., Dixon, T. H., Malservisi, R., Jiang, Y., Protti, M., & Muller, C. (2020). Slow slip and inter-transient locking on the Nicoya megathrust in the late and early stages of an earthquake cycle. *Journal of Geophysical Research: Solid Earth*, *125*(11), e2020JB020503. https://doi.org/10.1029/2020JB020503

Yue, H., Lay, T., Schwartz, S. Y., Rivera, L., Protti, M., Dixon, T. H., et al. (2013). The 5 September 2012 Nicoya, Costa Rica Mw 7.6 earthquake rupture process from joint inversion of high-rate GPS, strong-motion, and teleseismic P wave data and its relationship to adjacent plate boundary interface properties. *Journal of Geophysical Research: Solid Earth*, *118*(10), 5453–5466. https://doi.org/10.1002/jgrb.50379